

Efficient Radar Modulation Recognition via a Noise-Aware Ensemble Neural Network

Do-Hyun Park, *Graduate Student Member, IEEE*, Min-Wook Jeon, *Graduate Student Member, IEEE*, Jinwoo Jeong, Isaac Sim, Sangbom Yun, Junghyun Seo, and Hyoung-Nam Kim, *Member, IEEE*,

Abstract—Electronic warfare support (ES) systems intercept adversary radar signals and estimate various types of signal information, including modulation schemes. The accurate and rapid identification of modulation schemes under conditions of very low signal power remains a significant challenge for ES systems. This paper proposes a recognition model based on a noise-aware ensemble learning (NAEL) framework to efficiently recognize radar modulation schemes in noisy environments. The NAEL framework evaluates the influence of noise on recognition and adaptively selects an appropriate neural network structure, offering significant advantages in terms of computational efficiency and recognition performance. Furthermore, we employ feature extraction blocks to enhance the efficiency of the proposed recognition model. We present the analysis results of the recognition performance of the proposed model based on experimental data. Our recognition model demonstrates superior recognition accuracy with low computational complexity compared to conventional classification models.

Index Terms—Electronic warfare support, modulation recognition, low probability of intercept, ensemble learning, convolutional neural network

I. INTRODUCTION

MODULATION recognition is a key task for identifying the characteristics of unknown received signals and is widely employed in both civilian and military fields. In civilian applications, modulation recognition techniques are primarily aimed at communication signals and are extensively used in cognitive radio and spectrum surveillance [1]–[3]. In military applications, modulation recognition is used in electronic warfare support (ES) systems. ES systems estimate the parameter information of unknown radar signals, such as pulse width, time of arrival, center frequency, and modulation scheme. The acquired signal information can be used to identify the type of unknown emitter by comparison with a database stored in the emitter library of the ES systems. The process from signal reception to emitter identification in ES systems is illustrated in Fig. 1. By utilizing this emitter identification information, allied forces can engage in actions such as radio jamming or deception [4], [5].

Recently, many radar emitters utilize low-probability-of-intercept (LPI) radar, having properties that make detection by an opponent's intercept receiver less likely. Therefore, the intercept receivers of ES systems are required to recognize

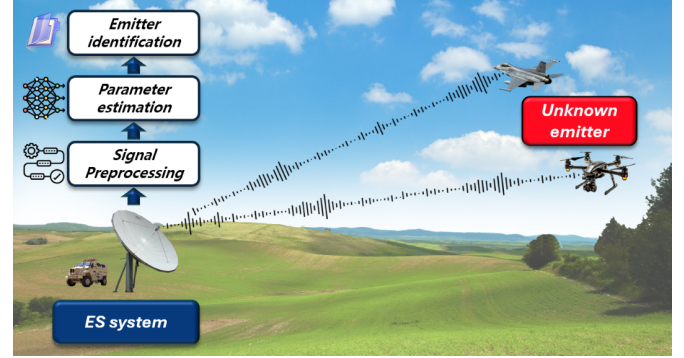


Fig. 1. Processes of the ES system for emitter identification.

the LPI radar modulation. Among the various features of LPI radars, the most prominent is their low signal-transmission power [5]. ES systems receive signals with very low signal-to-noise ratios (SNRs) because of their low transmission output. Consequently, extensive research has focused on the robust recognition of modulation schemes in low SNR environments.

In general, modulation recognition techniques involve two processes: signal representation and classification. Various techniques for signal representation include features such as power spectral density [6] and statistical feature extraction using the instantaneous phase and frequency [7]. In addition, time-frequency images (TFIs), such as the short-time Fourier transform [8], Wigner-Ville distribution (WVD) [5], [6], [9], and Choi-Williams distribution (CWD) [5], [6], [10]–[15] are often used. The classification process uses hierarchical decision trees [7], [8], [16], support vector machines [17], [18], and a multilayer perceptron (MLP) [5], [6], [9]–[11], [13]–[15] to classify the modulation scheme. Recently, convolutional neural network (CNN) models that use convolution layers to extract spatial features from TFIs and employ an MLP (or fully connected layers) for modulation scheme classification have shown improved recognition performance compared with conventional methods, especially in environments with low SNR [9], [11], [14].

The conventional CNN-based modulation recognition technique follows the algorithm flowchart shown in Fig. 2(a). First, a TFI was generated from the received signals, and the spatial features were extracted using convolution layers. During the feature extraction process, the depth of the features extracted by each convolution layer varied. In the initial convolution layers, basic low-level features such as corners and edges were extracted from the input image. In the later stages, these basic

Do-Hyun Park, Min-Wook Jeon, and Hyoung-Nam Kim are with the School of Electrical and Electronics Engineering, Pusan National University, Busan 46241, Republic of Korea.

Jinwoo Jeong, Isaac Sim, Sangbom Yun, and Junghyun Seo are with the LIG Nex1, Seongnam-si 13488, Republic of Korea.

features led to the extraction of more complex and abstract mid- and high-level features based on cumulative knowledge from earlier stages [19]. Finally, a classifier comprising fully connected layers used the extracted features to determine the modulation scheme.

Because ES systems must immediately estimate the information of the received signals, the use of lightweight CNN models is imperative. Considerable research has been conducted on CNN models that efficiently extract modulation features with low computational complexity while maintaining high recognition accuracy. CNNs that use depth-wise convolution are acknowledged to be more efficient than conventional CNNs, and such models have demonstrated the ability to efficiently classify unknown signal modulation schemes [20]–[23]. The neural architecture search (NAS) technique has drawn attention for its ability to automatically design optimized neural network structures, thereby maximizing efficiency and performance in processing complex and varied data [24], [25]. The application of the NAS technique in the field of radar modulation recognition has demonstrated its potential for designing efficient recognition models [26], [27]. In addition, a channel-shuffling technique designed to enhance the learning capabilities and parameter efficiency of neural networks has been proposed, and classification models utilizing this technique have shown excellent performance in modulation recognition [28]–[30].

Although existing CNN-based models exhibit efficiency in radar modulation recognition, a significant issue with these models is their substantial decrease in performance in low SNR environments. This decrease occurred because they employed structures with limited feature extraction capabilities to reduce the computational load. This issue can be addressed by increasing the computational complexity of the recognition model. However, recognition models applied to ES systems need to estimate signal parameters instantaneously. In high SNR environments, recognition models that enhance feature extraction capabilities with a high computational load can result in unnecessary power consumption and excessively long inference times. Consequently, existing models that use fixed neural network architectures generate unnecessary computations in low-noise environments or exhibit insufficient recognition capabilities in high-noise environments.

This study proposes a novel neural network architecture to address these issues, as depicted in Fig. 2(b). The proposed architecture exploits a noise-aware ensemble learning (NAEL) technique that evaluates the influence of noise on recognition and adaptively adjusts the network structure accordingly. The proposed model initially utilizes a lightweight preliminary recognizer to perform modulation recognition. When the recognition outcomes of the preliminary recognizer are compromised by noise interference, an advanced recognizer capable of extracting deeper features is employed to determine the final modulation recognition outcomes. By employing a conditional decision-making model with this noise-aware approach, unnecessary computation in high SNR environments can be reduced, while recognition accuracy in low SNR environments is enhanced.

The primary objective of this study is to advance ES

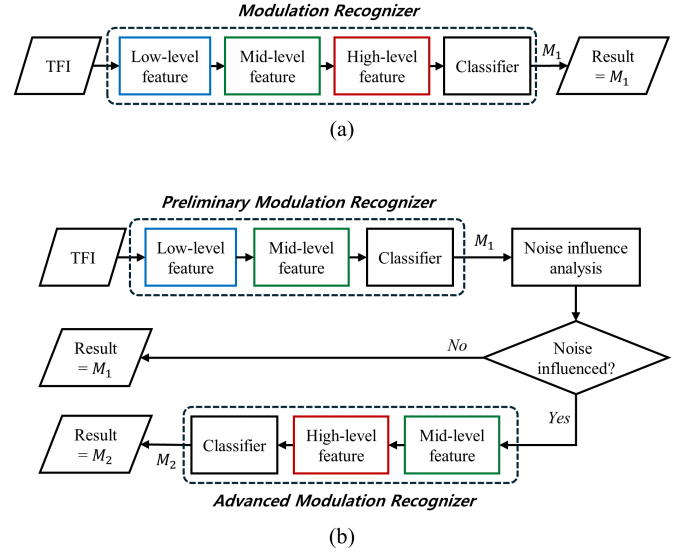


Fig. 2. Flow charts of modulation recognition models based on CNN: (a) conventional CNN architecture for modulation recognition, (b) proposed CNN architecture for modulation recognition.

systems by introducing an efficient neural network architecture that utilizes a novel method to evaluate the influence of noise on recognition decisions. This study demonstrates that integrating a noise-aware method can substantially enhance recognition accuracy compared to existing models and address the challenges posed by high power consumption in deep-learning models. The major contributions of this study are summarized as follows:

- We introduce a recognition model based on spatial feature extraction (FE) blocks that achieve high modulation recognition performance with low computational load. Our model also incorporates a data-reuse strategy to further enhance efficiency.
- We propose a novel methodology for evaluating the impact of noise on modulation recognition. Furthermore, we propose the NAEL framework, which adaptively selects the optimal neural network structure based on the noise influence on recognition.
- Through performance analysis using real measured data, we demonstrate that our proposed model outperforms and is more efficient than existing CNN models.

The remainder of this paper is organized as follows: In Section II, we introduce the intercepted radar signal model and the time-frequency analysis method. Section III outlines the proposed modulation recognition model and a method for assessing the significance of noise in recognition results using a noise-aware network. The results of analyzing the performance and computational loads of the proposed model compared to existing models are provided in Section IV, and Section V presents our conclusions.

TABLE I
FREQUENCY AND PHASE MODULATION FUNCTIONS FOR 12 MODULATION SCHEMES.

Scheme	$f(n)$	$\phi(n)$
LFM	$f_c + n \frac{B}{\tau_{pw}} T_s$	ϕ_0
Costas	f_{cs}	ϕ_0
BPSK	f_c	0 or π
Frank ¹	f_c	$\frac{2\pi}{M}(i-1)(j-1)$
P1 ¹	f_c	$-\frac{\pi}{M}[M-(2j-1)][(j-1)M+i-1]$
P2 ¹	f_c	$-\frac{\pi}{2M}(2i-1-M)(2j-1-M)$
P3 ²	f_c	$\frac{\pi}{N_c}(i-1)^2$
P4 ²	f_c	$\frac{\pi(i-1)^2}{N_c} - \pi(i-1)$
T1 ³	f_c	$\frac{2\pi}{N_{ps}} \left[(N_g n T_s - i \tau_{pw}) \frac{i N_{ps}}{\tau_{pw}} \right] \bmod 2\pi$
T2 ³	f_c	$\frac{2\pi}{N_{ps}} (N_g n T_s - i \tau_{pw}) \left(\frac{2i - N_g + 1}{\tau_{pw}} \right) \frac{N_{ps}}{2} \bmod 2\pi$
T3	f_c	$\frac{2\pi}{N_{ps}} \left(\frac{N_{ps} B (n T_s)^2}{2 \tau_{pw}} \right) \bmod 2\pi$
T4	f_c	$\frac{2\pi}{N_{ps}} \left(\frac{N_{ps} B (n T_s)^2}{2 \tau_{pw}} - \frac{N_{ps} B n T_s}{2} \right) \bmod 2\pi$

¹ $i = 1, 2, \dots, M$, $j = 1, 2, \dots, M$

² $i = 1, 2, \dots, N_c$

³ $i = 1, 2, \dots, n-1$

II. SIGNAL MODEL AND PREPROCESSING

A. Intercepted Radar Signal

The discrete-time complex radar signal $y(n)$ intercepted by the ES receiver can be expressed as

$$y(n) = x(n) + w(n) = A \exp(j2\pi f(n)t + \phi(n)) + w(n) \quad (1)$$

where $x(n)$ represents the complex envelopes of the transmitted radar signals, $w(n)$ represents the complex additive white Gaussian noise, A is the amplitude, and $f(n)$ and $\phi(n)$ are the frequency and phase modulation functions, respectively.

Various modulation techniques can be employed for the radar waveform design. We considered two frequency modulations (FM) and ten phase modulations (PMs), for a total of 12 modulation schemes for recognition. Specifically, linear FM (LFM) and Costas codes were considered for the FM, and binary phase-shift keying (BPSK), polyphase codes (Frank, P1, P2, P3, and P4), and polytime codes (T1, T2, T3, and T4) were considered for the PM. For the BPSK signal included in the PM, the Barker code was used for the binary code of BPSK.

The phase $\phi(n)$ in (1) is kept constant with respect to the initial phase ϕ_0 for FM radar signals, whereas the frequency $f(n)$ is kept constant at the center frequency f_c for PM radar signals. Table I describes $f(n)$ and $\phi(n)$ for the 12 modulation schemes considered in this study, while Table II presents the definitions of the parameters used in Table I.

B. Time-frequency Analysis

Rather than using the intercepted signal $y(n)$ directly for modulation recognition, $y(n)$ is preprocessed before being

TABLE II
NOTATION AND DEFINITIONS FOR MODULATION FUNCTIONS

Notation	Definition
f_c	Carrier frequency
ϕ_0	Initial phase
B	Bandwidth of signal
τ_{pw}	Pulse width
T_s	Sampling period
f_{cs}	Costas frequency sequence
A mod B	Remainder of dividing A by B
M	Number of frequency steps
N_c	Number of subcodes
N_{ps}	Number of phase states
N_g	Number of segments

fed into a neural network to improve recognition performance. Among various signal representation methods, transforming the intercepted signal into a time-frequency image can significantly enhance recognition performance by effectively capturing radar modulation characteristics. As described in Section I, various time-frequency analysis methods can be employed. This study utilizes the Choi-Williams distribution (CWD), renowned for its exceptional time-frequency analysis performance using an exponential kernel to minimize cross-term components. The continuous CWD of the input signal $y(t)$ is given by [31]

$$\text{CWD}(t, f) = \int_{-\infty}^{\infty} \exp(-j\omega\tau) \int_{-\infty}^{\infty} \sqrt{\frac{\sigma}{4\pi\tau^2}} \exp\left(-\frac{(\mu-t)^2}{4\tau^2/\sigma}\right) y\left(\mu + \frac{\tau}{2}\right) y^*\left(\mu + \frac{\tau}{2}\right) d\mu d\tau \quad (2)$$

where t and f are the time and frequency variables, respectively, $\omega = 2\pi f$ is the angular frequency, and σ ($\sigma > 0$) is a scaling factor determining the trade-off between cross-term suppression and frequency resolution. In this study, we set σ to 1 for CWD time-frequency analysis.

III. PROPOSED MODULATION RECOGNITION MODEL

This section describes the proposed modulation recognition model exploiting the NAEL framework. Fig. 3 illustrates the overall neural network architecture of our proposed recognition model. The model consists of three neural networks: a preliminary recognition network (PRN), noise-aware network (NAN), and advanced recognition network (ARN). A brief description of each network is provided below.

- The PRN primarily determines the modulation recognition results from the TFI.
- The NAN assesses whether the modulation recognition results derived by the PRN are affected by noise.
- To mitigate potential noise-induced misrecognition, the NAEL framework utilizes the ARN, which excels in precise feature extraction, to make the final decision. This occurs when the NAN determines that recognition results are likely to be significantly influenced by noise.

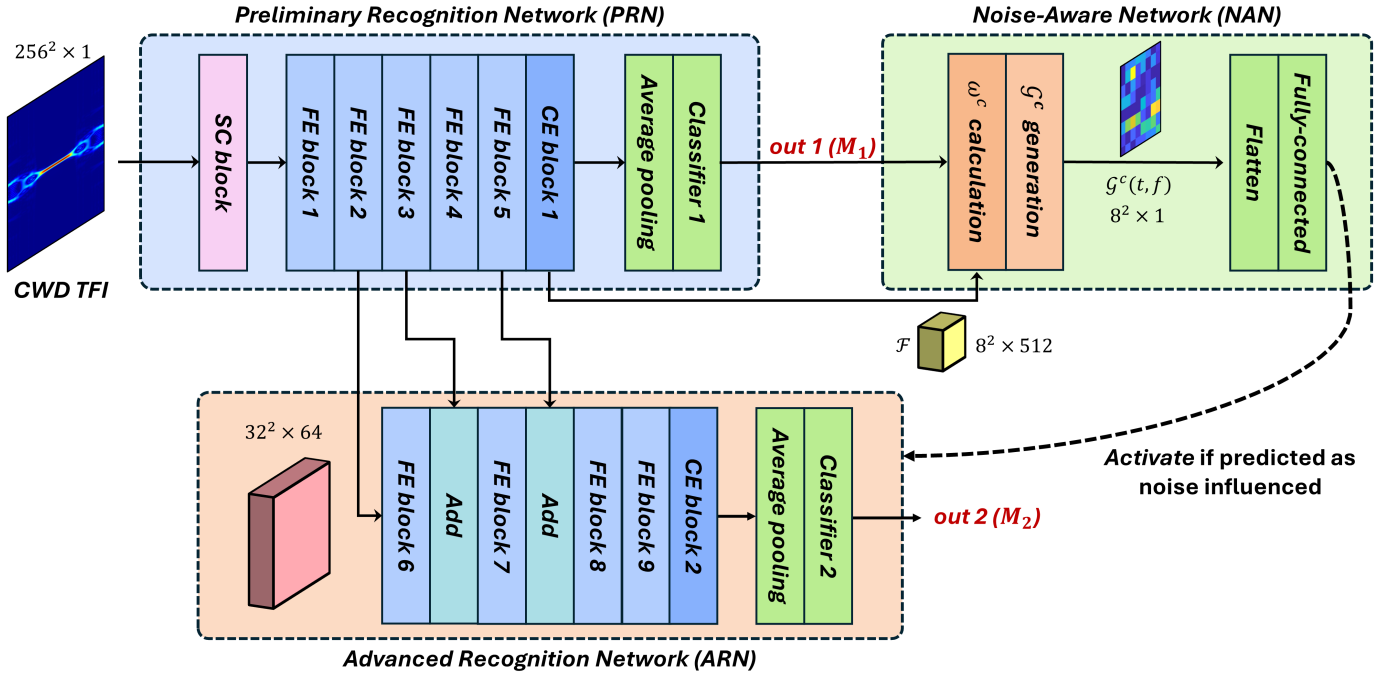


Fig. 3. Overall architecture of the NAEL framework. Our proposed recognition model uses SC, FE, and CE blocks to produce feature maps and compute importance weights w^c culminating in the creation of a gradient map G^c .

A. FE Block

The PRN and ARN within the NAEL framework utilize FE blocks that are both powerful and computationally efficient, unlike techniques used in conventional CNNs, where spatial features are extracted from the input feature map using standard convolution (SC) layers. The output feature map of a SC operation F_{os} is calculated as:

$$F_{os}(h, w, c_o) = \sum_{i,j,c_i} K_s(i, j, c_i, c_o) \cdot F_i(h+i-1, w+j-1, c_i) \quad (3)$$

where K_s represents the SC kernel and F_i is the input feature map. The dimensions of F_i , F_{os} , and K_s are $H_f \times W_f \times C_i$, $H_f \times W_f \times C_o$, and $H_k \times W_k \times C_i \times C_o$, respectively. Here, H_f represents the height of the feature map, W_f the width of the feature map, C_i the number of input feature map channels, C_o the number of output feature map channels, H_k the height of the kernel, and W_k the width of the kernel. By padding the input feature map with zeros and setting the stride to 1, the convolution operation moves the kernel one step at a time, resulting in an output feature map (F_{os}) of the same height and width as the input feature map (F_i). As shown in (3), the SC layer applies a distinct filter to each input feature map channel. The computational cost of a SC operation is expressed as

$$H_k \cdot W_k \cdot C_i \cdot C_o \cdot H_f \cdot W_f. \quad (4)$$

To reduce the computational cost of extracting spatial features, we decomposed the SC operation into two steps: depth-wise and point-wise convolution operations. Unlike standard convolution, which uses multiple filters (one for each output channel) that span all input channels, depth-wise convolution employs a single filter per input channel. The feature-map out-

put of the depth-wise convolution operation F_{od} is expressed as follows:

$$F_{od}(h, w, c_i) = \sum_{i,j} K_d(i, j, c_i) \cdot F_i(h+i-1, w+j-1, c_i) \quad (5)$$

where K_d denotes the depth-wise convolution kernel with dimensions $H_k \times W_k \times C_i$. Each channel operation in (5) uses a corresponding filter from K_d , generating an output channel in F_{od} . Thus, the number of channels in F_i and F_{od} remains the same. Following depth-wise convolution, a point-wise convolution with a 1×1 kernel combines the channels of F_{od} to produce C_o output channels. The total computational complexity of depth-wise and point-wise convolutions is expressed as follows:

$$H_k \cdot W_k \cdot C_i \cdot H_f \cdot W_f + C_i \cdot C_o \cdot H_f \cdot W_f \quad (6)$$

where the first term represents the computational cost of depth-wise convolution, and the second term represents the cost of point-wise convolution. This method of factorizing SC into two operations significantly reduces computational complexity while maintaining high spatial feature extraction performance [20], [32].

Our proposed recognition neural network employs FE blocks following the structures illustrated in Figs. 4 and 5. The structure depicted in Fig. 4 is used repetitively from the second stage onward, while the structure in Fig. 5 is used only in the first stage. In the first stage, depending on the parameters used in the block design, the model can adjust the number of output channels, perform downsampling, or both simultaneously.

As shown in Fig. 4, a feature map input into the FE block undergoes channel expansion by a factor α through a 1×1 point-wise convolution. Subsequently, spatial features were

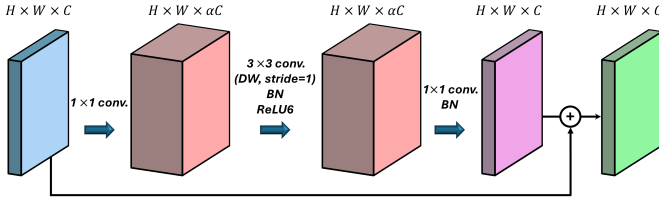


Fig. 4. Block diagram illustrating the structure used in the FE block, excluding the first stage.

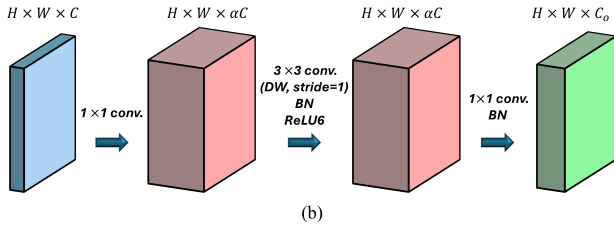
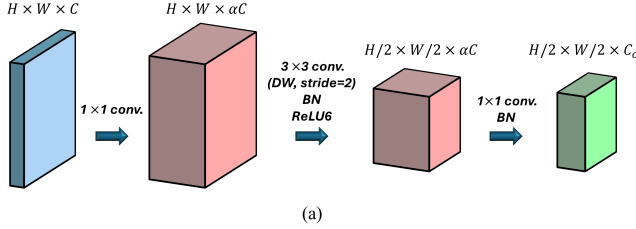


Fig. 5. Block diagrams illustrating the structures corresponding to the first stage of the FE block. Structure performing (a) both channel adjustment and downsampling operation, (b) only channel adjustment.

extracted using depth-wise convolution. Batch normalization (BN) is then applied to enhance training efficiency [33]. An activation function was employed to incorporate nonlinearity, enabling the neural network to learn complex patterns. Typically, CNNs use the ReLU activation function [34] due to its simplicity and computational efficiency. We used a variant called ReLU6, which limits activations to the range of 0 to 6, thereby enhancing network robustness [20]. After applying the activation function, a 1×1 point-wise convolution layer combined the outputs of the depth-wise convolution. The number of output channels from this convolution layer is adjusted to match the input feature map dimensions. Finally, a skip connection adds the initial input feature map to the output, producing the final output feature map. An FE block with this structure has the following advantages:

- 1) By expanding channels for spatial feature extraction and subsequently compressing them, this method reduces parameter usage and computational complexity.
- 2) Introducing skip connections between the input and output feature maps helps mitigate learning difficulties that can arise with deep network architectures.
- 3) The FE block processes inputs and outputs with a reduced number of channels. This approach contrasts with traditional CNN structures [35], which typically employ wide-channel feature maps for skip connections. Using fewer channels for skip connections significantly reduces memory usage in our model.

Downsampling operations can be integrated into the first

TABLE III
DETAILED STRUCTURE OF THE RECOGNITION NETWORKS WITHIN THE NAEL FRAMEWORK

Network	Block	Input	C_o	α	r	s
PRN	SC block	$256^2 \times 1$	32	-	1	2
	FE block 1	$128^2 \times 32$	32	4	2	2
	FE block 2	$64^2 \times 32$	64	4	3	2
	FE block 3	$32^2 \times 64$	64	4	4	2
	FE block 4	$16^2 \times 64$	96	4	3	1
	FE block 5	$16^2 \times 96$	128	4	3	2
ARN	CE block 1	$8^2 \times 128$	512	-	1	1
	FE block 6	$32^2 \times 64$	64	6	5	2
	FE block 7	$16^2 \times 64$	128	6	5	2
	FE block 8	$8^2 \times 128$	256	6	5	2
	FE block 9	$4^2 \times 256$	512	6	5	1
	CE block 2	$4^2 \times 512$	1024	-	1	1

stage of the FE block to enhance computational efficiency and extract key features effectively. If the block parameters are set to include a downsampling operation, the structure illustrated in Fig. 5(a) is used. This structure reduces the spatial dimensions of the output feature map by half and adjusts the number of output channels to C_o . In contrast, the structures illustrated in Fig. 5(b) is used. Here, the FE block retains the original spatial dimensions of the input feature map while adjusting the number of output channels to C_o .

B. Modulation Recognition Neural Networks

This subsection provides a detailed explanation of the structures of PRN and ARN that constitute the proposed recognition model. PRN and ARN utilize FE blocks for modulation recognition. Table III summarizes the input dimensions and parameters used for each block, where C_o denotes the number of channels in the block output, r represents the number of repetitions for spatial feature extraction, and s indicates the convolution layer stride in the first stage of the block. For the FE block, the structure shown in Fig. 5 is used in the first stage, and the structure in Fig. 4 is repeated $r - 1$ times for subsequent stages. In addition, if $s = 2$, the structures shown in Fig. 5(a) is used in the first stage; if $s = 1$, the structure in Fig. 5(b) is used. Based on our experimental results, setting the parameters listed in Table III yielded the best modulation recognition performance.

As shown in Fig. 3, PRN initially extracts features from the input TFI using a SC block. The first neural network process involved extracting significant low-level features. In the initial stage of the PRN, we used a standard 3×3 convolution layer, followed by BN and ReLU6 activation functions. This SC block effectively captures basic features from the input data. We then utilized FE blocks based on depth-wise convolution in the subsequent stages.

For classification, transforming a feature map into a one-dimensional feature vector is crucial for effective processing by a classifier based on fully connected layers. To achieve this, we employed a channel-expansion (CE) block after the last FE block. This block consists of a 1×1 convolution layer, followed by BN and ReLU6 activation. The CE block enhances

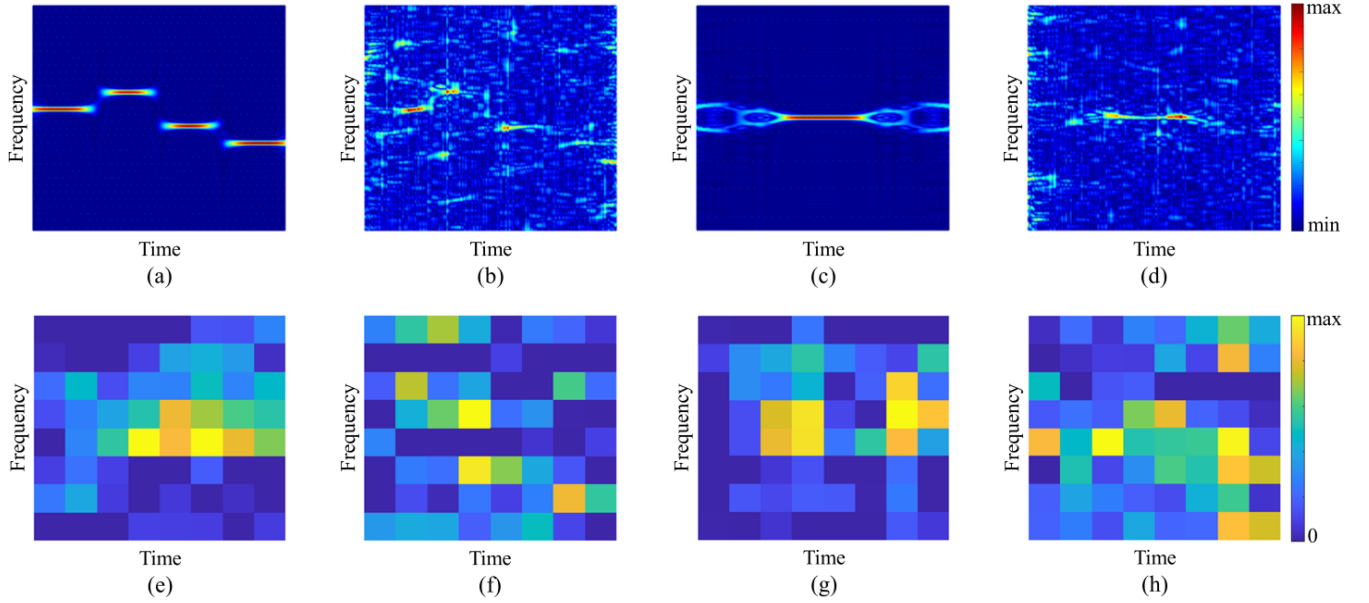


Fig. 6. Examples of TFIs and gradient maps for Costas and T2 code simulated signals; (a) and (c) TFIs of transmitted Costas and T2 code signals, (b) and (d) TFIs of received Costas and T2 code signals, (e) and (g) gradient maps for the correctly classified cases of Costas and T2 codes, (f) and (h) gradient maps for the misclassified cases of Costas and T2 codes.

the representation of each channel in \mathcal{F} , the output of the last FE block, to capture essential information. Subsequently, a one-dimensional feature vector is produced by averaging the values across channels of the CE block output. This feature vector is then fed into a classifier composed of fully connected layers followed by a softmax layers. The classifier computes class scores based on the feature vector, identifying the modulation scheme with the highest score.

In cases where the NAN determines significant noise influence on PRN's recognition results (as explained in a subsequent subsection), ARN is activated for more precise analysis. Although both ARN and PRN utilize FE blocks for spatial feature extraction, ARN differs from PRN in the following ways:

- 1) The ARN employs FE blocks with a higher channel expansion ratio α compared to the PRN, facilitating more detailed feature extraction.
- 2) Through the extraction of higher-level features, ARN generates final feature maps that are reduced in spatial dimensions but increased in channel depth compared to those of the PRN.
- 3) As illustrated in Fig. 3, some of the inputs to ARN's FE blocks include outputs from the PRN block. This data-reuse strategy enhances the efficiency of the modulation recognition model design.

C. Noise-Aware Neural Network

A key proposal of this study involves using a noise-aware method to determine the impact of noise on recognition results derived by the PRN. To achieve this, the NAN generates a gradient map illustrating the regions of the input TFI on which the PRN focuses to derive modulation recognition results. The method for generating the gradient map is based on

computing gradient information from the PRN's feature map \mathcal{F} as gradient information is crucial for visually highlighting the data influencing the decision [36]. To obtain the gradient map, the process starts by computing the gradient between the c -th class score y^c (the highest among computed class scores) from the PRN's classifier output, and the k -th channel of the feature map \mathcal{F}^k from the output of the PRN's CE block. This gradient $\partial y^c / \partial \mathcal{F}^k$ represents the influence of \mathcal{F}^k on y^c . To determine the importance of the k -th feature map channel for the c -th class score, importance weights for the k -th channel $w^c(k)$ are computed using global average pooling across the width and height dimensions of \mathcal{F}^k . This process is summarized as follows:

$$w^c(k) = \frac{1}{H \times W} \sum_{t_i=1}^H \sum_{t_j=1}^W \frac{\partial y^c}{\partial \mathcal{F}^k(t_i, f_j)} \quad (7)$$

where H and W denote the height and width of \mathcal{F} , and $\mathcal{F}^k(t_i, f_j)$ are the feature map values for the i -th height and j -th width at the k -th channel.

By performing a weighted sum on \mathcal{F}^k with the importance weights and applying the ReLU activation function, a gradient map \mathcal{G}^c is produced. This gradient map provides a visual explanation for the recognition basis of the c -th modulation scheme as follows:

$$\mathcal{G}^c(t, f) = \text{ReLU} \left(\sum_k \mathcal{F}^k(t, f) \cdot w^c(k) \right). \quad (8)$$

Fig. 6 shows examples of gradient maps for simulated signals in cases of correct classification and misclassification. Costas and T2 code signals were used in an environment with an SNR of -11 dB. In the proposed recognition model, the feature map \mathcal{F} has dimensions of 8×8 , resulting in a gradient map of the same 8×8 size. As shown in Fig. 6(e) and (g),

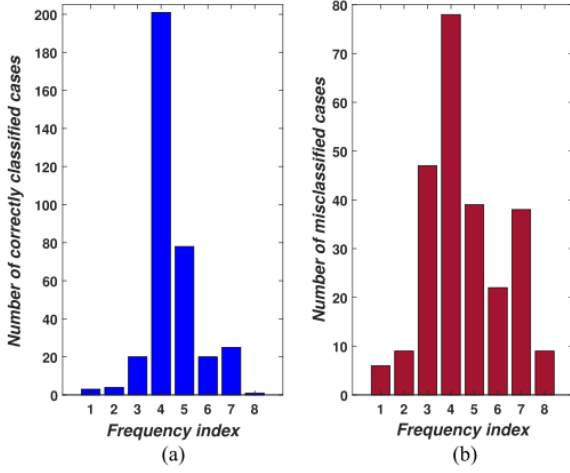


Fig. 7. Distribution of the f_{max} for the two cases: (a) correctly classified case, and (b) misclassified case.

during correct classification, the gradient map exhibits the highest values at indices 4 and 5 in the frequency domain, corresponding to the signal's center frequency. The ES system was assumed to accurately estimate the center frequency for all simulated signals before performing modulation recognition, with a frequency offset applied to align the center frequency with the middle of the TFI frequency axis. In case of misclassification, as shown in Fig. 6(f) and (h), high values appear at positions other than the center frequency. This occurs because the gradient map highlights noisy areas where the signal does not exist, leading the PRN to focus on noise and make incorrect decisions.

Fig. 7 shows the distribution of frequency domain values at the highest points in the gradient maps for both correctly and incorrectly classified cases. For this analysis, 50 simulated signals for each of the 12 modulation schemes were generated in an environment with an SNR of -15 dB. The frequency index f_{max} of the highest point in $\mathcal{G}^c(t, f)$ was extracted as follows:

$$f_{max} = \arg \max_f \left(\sum_{t=1} \mathcal{G}^c(t, f) \right). \quad (9)$$

As seen in Fig. 7(a), which shows the distribution of f_{max} when correctly classified, the highest values are concentrated at frequency indices 4 and 5, corresponding to the center frequency. In contrast, Fig. 7(b), which depicts the distribution when misclassified, shows significantly more outliers compared to the correct classification case. These results indicate that using a gradient map can be highly effective in assessing the reliability of recognition results.

Gradient maps serve as visualizations of the neural network's decision-making process, allowing for the diagnosis of faults using this explainability. The proposed model uses a gradient map to determine whether current recognition results are significantly affected by noise. Fig. 7 demonstrates the usefulness of the gradient map using f_{max} ; however, a deep-learning-based classifier that utilizes all elements of the gradient map as input can achieve better noise awareness

TABLE IV
MODULATION PARAMETERS FOR DATASET GENERATION

Scheme	Param.	Value
All schemes	SNR (dB)	$U(-15, 5)$
LFM	f_c	$U(1/8f_s, 1/4f_s)$
	B	$U(1/20f_s, 1/8f_s)$
Costas	f_{min}	$U(1/40f_s, 1/10f_s)$
	L_{hs}	$\{4, 6\}$
	f_{hop}	$U(1/40f_s, 3/40f_s)$
Barker	f_c	$U(1/8f_s, 1/4f_s)$
	L_B	$\{7, 11, 13\}$
	N_{sc}	$\{20, 24, 28, 32\}$
Frank, P1	f_c	$U(1/8f_s, 1/4f_s)$
	N_{sc}	$\{5, 6, 7\}$
	M	$\{6, 7, 8\}$
P2	f_c	$U(1/8f_s, 1/4f_s)$
	N_{sc}	$\{5, 6, 7\}$
	M	$\{6, 8\}$
P3, P4	f_c	$U(1/8f_s, 1/4f_s)$
	N_{sc}	$\{5, 6, 7\}$
	N_c	$\{36, 49, 64\}$
T1, T2	f_c	$U(1/8f_s, 1/4f_s)$
	k	$\{5, 6, 7\}$
T3, T4	f_c	$U(1/8f_s, 1/4f_s)$
	ΔF	$U(1/20f_s, 1/10f_s)$

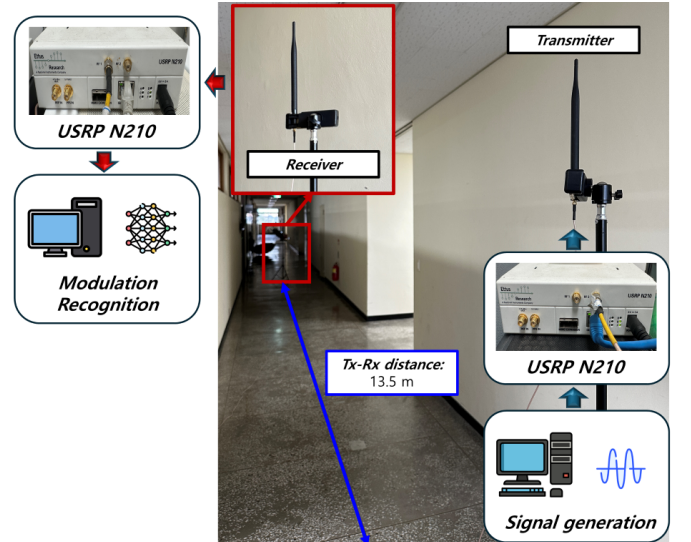


Fig. 8. Measurement environment for constructing test datasets.

performance. To this end, we flattened the gradient map into a one-dimensional gradient vector of size 64×1 . Subsequently, a classifier consisting of fully connected and softmax layers predicts whether the recognition is affected by noise.

IV. PERFORMANCE ANALYSIS

This section presents the modulation recognition performance of the classification model based on the NAEL framework. Additionally, we provide a comparative performance analysis of the proposed and existing classification models. For the performance analysis, a training dataset was generated in a simulation environment, and a test dataset was produced using real measured signals.

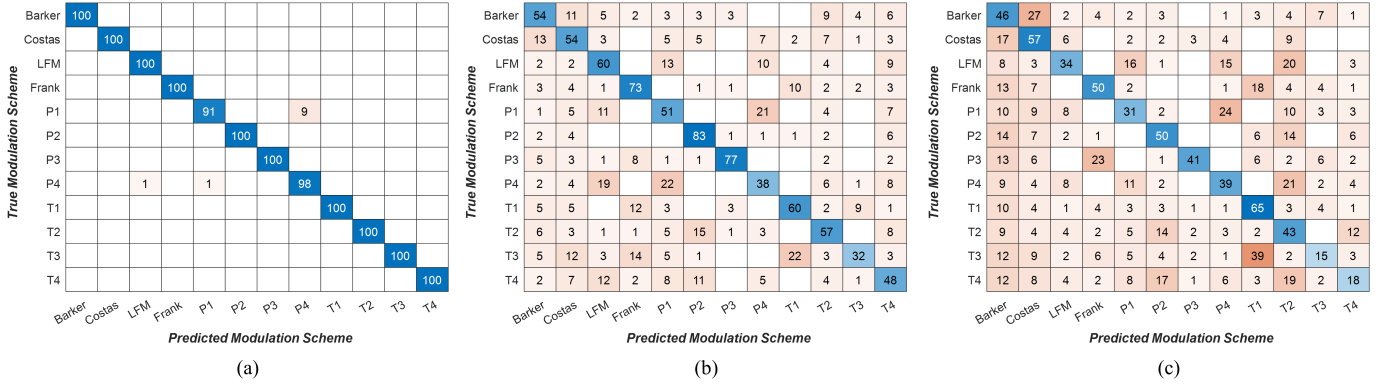


Fig. 9. Confusion matrix of the proposed recognition model using the test dataset collected in the (a) first scenario, (b) second scenario (low transmit power), and (c) third scenario (very low transmit power).

A. Training Recognition Model

A training dataset was built to train the recognition model, generating 5,000 simulated signals for each of the 12 modulation schemes. Table IV lists the parameters used in the signal generation, where f_s , f_{min} , L_{hs} , f_{hop} , L_B , and N_{sc} represent sampling frequency, fundamental frequency of the Costas code, hopping sequence length of the Costas code, frequency spacing of the Costas code, length of the Barker code, and the number of samples per carrier frequency cycle, respectively. Additionally, $U(\cdot, \cdot)$ denotes a uniform distribution.

The proposed NAEL framework consists of three neural networks, each trained individually whereas keeping the weights of the other networks constant during training. For the performance analysis, all classification models used in this study, including the NAEL-based model, were trained using the Adam optimizer [37]. Training was conducted for 100 epochs, resulting in 187,500 weight updates. The input data fed into all neural networks were normalized to have a mean of 0 and a variance of 1.

B. Test Dataset Generation

The test dataset for performance analysis was constructed by collecting signals in a real-world environment, as shown in Fig. 8. Radar signals with 12 modulation schemes were generated using MATLAB. The generated digital signals were converted to analog signals using the USRP N210 software-defined radio platform [38]. The converted analog signals were transmitted via an antenna connected to a transmitting USRP N210 and received by an antenna connected to a distant receiving USRP N210. Vertical antennas were used for both transmission and reception, positioned 13.5 m apart. The radar signals used in this experiment had a center frequency of 1,902.5 MHz. The collected signals were digitized at a sampling rate of 10 MHz using a USRP N210 and imported into a computer for modulation recognition.

The signals were recorded for three different scenarios by varying the transmission power to analyze performance under various SNR conditions. In each scenario, 100 signals were collected for each of the 12 modulation schemes. One scenario with relatively high signal power and two scenarios with low signal power were used for the test dataset generation. The

estimated SNRs for the first, second, and third scenarios were approximately -4 , -15 , and -17 dB, respectively. Notably, in the experiments using the USRP, the exact SNR for each scenario could not be calculated. However, an approximate SNR can be estimated by assuming that the power of the collected signal $y(n)$ is the sum of the power of the signal $x(n)$ and that of the signal collected in an environment without transmitted signals (i.e., received data with only noise $w(n)$ presence).

C. Analysis Results on Experimental Data

In this subsection, we present the results of the performance analysis of the proposed model using the test dataset. Additionally, we compared the modulation recognition performance of the proposed model with existing models known for their high accuracy and efficiency despite their low computational complexity.

Fig. 9 shows the confusion matrix of the proposed model for the three different scenarios. A confusion matrix is a widely used metric that visually represents the difference between true labels and predicted results in classification problems. In the confusion matrix, the columns represent the actual transmitted modulation schemes, and the rows represent the predicted modulation schemes. The modulation recognition results were counted in the corresponding grids, and the total sum of all grids was 1,200 since 100 signals were collected for each modulation scheme.

In the first scenario (as seen in Fig. 9(a)), where the signal power is relatively high, the proposed recognition model exhibits low confusion, resulting in high classification performance. However, as shown in Fig. 9(b), many misclassifications occur as the SNR decreases. In particular, distinguishing between Frank and P3, as well as P1 and P4 is difficult, as analyzed in [15]. When the signal power was extremely low, the classification performance for all modulation schemes decreased, as shown in Fig. 9(c).

Fig. 10 presents the comparison results between the proposed model and existing classification models across the three scenarios. We used MNasNet [25], ShuffleNetV1 [28], ShuffleNetV2 [29], MobileNetV1 [20], and MobileNetV2 [21] for comparison. These models are known for their high accu-

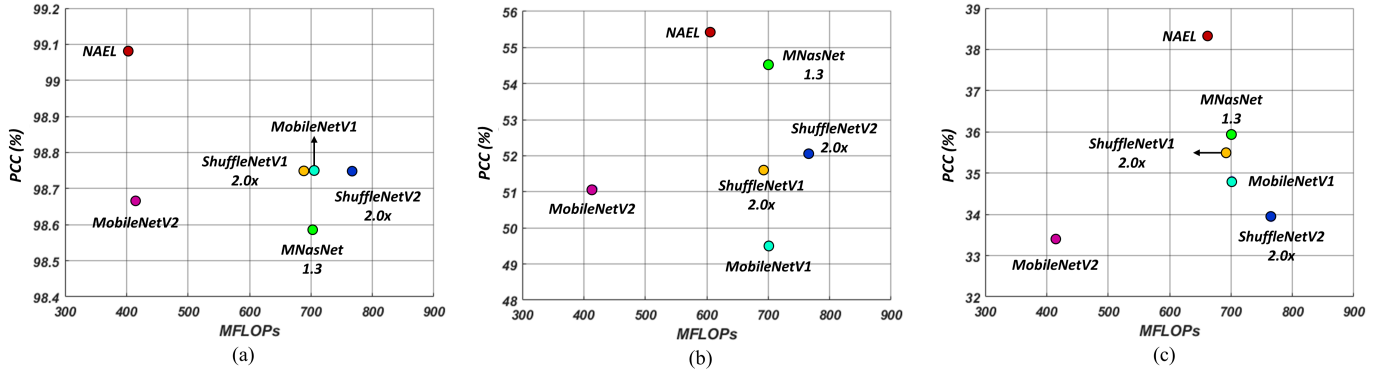


Fig. 10. Performance versus computational cost of various models using the test dataset collected in the (a) first scenario, (b) second scenario (low transmit power), (c) third scenario (very low transmit power).

racy and efficiency, as described in Section I. To evaluate the efficiency of each model, we used the probability of correct classification (PCC) versus mega floating point operations (MFLOPs). The computational load of the proposed recognition model varied with each inference; therefore, the average FLOPs were calculated for all 1,200 inferences.

In the high SNR scenario shown in Fig. 10(a), the proposed model exhibited the highest recognition performance and the lowest computational cost compared to the other models. This is because the NAN determined that most of the input data were not significantly affected by noise. Consequently, recognition could be performed using only the PRN at a relatively low computational cost, without activating the ARN. In fact, the NAN of our proposed model activated the ARN 20 times out of 1,200 predictions in the first scenario.

In a low SNR environment scenario, as shown in Fig. 10(b), the PCCs for all classification models are around 50%. Among them, our proposed model exhibits the highest classification performance compared to other models. The computational cost of our proposed model was also the lowest among those achieving high recognition accuracy within the comparison group. In the third scenario, with extremely low signal power as shown in Fig. 10(c), the PCCs of the classification models are around 35%. Here, the proposed model shows superior performance with a PCC approximately 2.5% higher than the best-performing comparison model. This is because the NAN identifies significant noise-affected data in the input, utilizing both PRN and ARN adaptively for the final decision. The proposed model also incurs lower computational costs. Efficiency is achieved by effectively using only the PRN for classification in cases where data are likely unaffected by noise, thereby avoiding unnecessary activation of ARN.

In summary, our recognition model demonstrates a lightweight structure in high SNR environments where precise classification may be unnecessary. Moreover, our model achieves excellent modulation recognition performance in low SNR environments with minimal increase in computational cost. These findings underscore the adaptability of the proposed NAEL framework to varying conditions, enabling efficient modulation recognition in real-world scenarios.

V. CONCLUSION

This study proposes NAEL, a deep-learning framework for radar modulation recognition that adaptively adjusts its model structure based on noise conditions. The NAEL framework utilizes efficient modulation classification networks with high feature extraction capabilities and low computational costs. A key component, the noise-aware network within NAEL, evaluates noise impact on recognition, allowing adaptive selection of neural network structures for varying noise levels. Experimental analysis demonstrates that the proposed model outperforms existing classification models in recognition accuracy across diverse noise environments. Moreover, the proposed model exhibits lower computational demands compared to alternatives, a distinction magnified under high signal powers. These results position the NAEL framework as promising for ES systems requiring efficient resource utilization, rapid inference speeds, high accuracy, reliability, and interpretability.

REFERENCES

- [1] S. Peng, S. Sun, and Y.-D. Yao, "A survey of modulation classification using deep learning: Signal representation and data preprocessing," *IEEE Transactions on Neural Networks and Learning Systems*, vol. 33, no. 12, pp. 7020-7038, Dec. 2022.
- [2] T. J. O'Shea, T. Roy, and T. C. Clancy, "Over-the-air deep learning based radio signal classification," *IEEE Journal of Selected Topics in Signal Processing*, vol. 12, no. 1, pp. 168-179, 2018.
- [3] S. Peng, H. Jiang, H. Wang, H. Alwageed, Y. Zhou, M. M. Sebdani, and Y.-D. Yao, "Modulation classification based on signal constellation diagrams and deep learning," *IEEE Transactions on Neural Networks and Learning Systems*, vol. 30, no. 3, pp. 718-727, 2019.
- [4] R. Wiley, *ELINT: The interception and analysis of radar signals*. Artech, 2006.
- [5] P. E. Pace, *Detecting and classifying low probability of intercept radar*. Artech House, 2009.
- [6] J. Lunden and V. Koivunen, "Automatic radar waveform recognition," *IEEE Journal of Selected Topics in Signal Processing*, vol. 1, no. 1, pp. 124-136, May 2007.
- [7] V. Iglesias, J. Grajal, P. Royer, M. A. Sanchez, M. Lopez-Vallejo, and O. A. Yeste-ojeda, "Real-time low-complexity automatic modulation classifier for pulsed radar signals," *IEEE Transactions on Aerospace and Electronic Systems*, vol. 51, no. 1, pp. 108-126, Jan. 2015.
- [8] G. Lopez-Risueno, J. Grajal, and A. Sanz-Osorio, "Digital channelized receiver based on time-frequency analysis for signal interception," *IEEE Transactions on Aerospace and Electronic Systems*, vol. 41, no. 3, pp. 879-898, Jul. 2005.
- [9] C. Wang, J. Wang, and X. Zhang, "Automatic radar waveform recognition based on time-frequency analysis and convolutional neural network," in *Proc. IEEE Int. Conf. Acoustics, Speech and Signal Processing (ICASSP)*, New Orleans, LA, USA, Mar. 2017, pp. 2437-2441.

- [10] E. R. Zilberman and P. E. Pace, "Autonomous time-frequency morphological feature extraction algorithm for LPI radar modulation classification," in *Proc. Int. Conf. Image Processing*, Atlanta, GA, USA, Oct. 2006, pp. 2321-2324.
- [11] T. Huynh-The, V.-S. Doan, C.-H. Hua, Q.-V. Pham, T.-V. Nguyen, and D.-S. Kim, "Accurate LPI radar waveform recognition with CWD-TFA for deep convolutional network," *IEEE Wireless Communications Letters*, vol. 10, no. 8, pp. 1638-1642, Aug. 2021.
- [12] M. Zhang, L. Liu, and M. Diao, "LPI radar waveform recognition based on time-frequency distribution," *Sensors*, vol. 16, no. 10, Article No. 1682, Oct. 2016.
- [13] M. Zhang, M. Diao, and L. Guo, "Convolutional neural networks for automatic cognitive radio waveform recognition," *IEEE Access*, vol. 5, pp. 11074-11082, Jun. 2017.
- [14] S.-H. Kong, M. Kim, L. M. Hoang, and E. Kim, "Automatic LPI radar waveform recognition using CNN," *IEEE Access*, vol. 6, pp. 4207-4219, Jan. 2018.
- [15] D.-H. Park, J.-H. Bang, J.-H. Park, and H.-N. Kim, "A fast and accurate convolutional neural network for LPI radar waveform recognition," in *Proc. 19th European Radar Conference (EuRAD)*, Milan, Italy, Sep. 2022, pp. 89-92.
- [16] E. E. Azzouz and A. K. Nandi, "Procedure for automatic recognition of analogue and digital modulations," *IEE Proceedings-Communications*, vol. 143, no. 5, pp. 259-266, Oct. 1996.
- [17] C.-S. Park and D. Y. Kim, "A novel robust feature of modulation classification for reconfigurable software radio," *IEEE Transactions on Consumer Electronics*, vol. 52, no. 4, pp. 1193-1200, Nov. 2006.
- [18] T. S. Tabatabaei, S. Krishnan, and A. Anpalagan, "SVM-based classification of digital modulation signals," in *Proc. IEEE Int. Conf. Systems, Man, and Cybernetics*, Istanbul, Turkey, Oct. 2010, pp. 277-280.
- [19] M. D. Zeiler and R. Fergus, "Visualizing and understanding convolutional networks," in *Proc. European Conf. Computer Vision (ECCV)*, Zurich, Switzerland, Sep. 2014, pp. 818-833.
- [20] A. G. Howard, M. Zhu, B. Chen, D. Kalenichenko, W. Wang, T. Weyand, M. Andreetto, and H. Adam, "MobileNets: Efficient convolutional neural networks for mobile vision applications," *arXiv preprint arXiv:1704.04861*, 2017. [Online]. Available: <https://arxiv.org/abs/1704.04861>
- [21] M. Sandler, A. Howard, M. Zhu, A. Zhmoginov, and L.-C. Chen, "MobileNetV2: Inverted residuals and linear bottlenecks," in *Proc. IEEE/CVF Conf. Computer Vision and Pattern Recognition (CVPR)*, Salt Lake City, UT, USA, Jun. 2018, pp. 4510-4520.
- [22] C. Xiao, S. Yang, and Z. Feng, "Complex-valued depthwise separable convolutional neural network for automatic modulation classification," *IEEE Transactions on Instrumentation and Measurement*, vol. 72, pp. 1-10, 2023.
- [23] G. B. Tunze, T. Huynh-The, J.-M. Lee, and D.-S. Kim, "Sparsely connected CNN for efficient automatic modulation recognition," *IEEE Transactions on Vehicular Technology*, vol. 69, no. 12, pp. 15557-15568, 2020.
- [24] B. Zoph, V. Vasudevan, J. Shlens, and Q. V. Le, "Learning transferable architectures for scalable image recognition," in *Proc. IEEE/CVF Conf. Computer Vision and Pattern Recognition (CVPR)*, Salt Lake City, UT, USA, Jun. 2018, pp. 8697-8710.
- [25] M. Tan, B. Chen, R. Pang, V. Vasudevan, M. Sandler, A. Howard, and Q. V. Le, "MnasNet: Platform-aware neural architecture search for mobile," in *Proc. IEEE/CVF Conf. Computer Vision and Pattern Recognition (CVPR)*, Long Beach, CA, USA, Jun. 2019, pp. 2815-2823.
- [26] X. Zhang, H. Zhao, H. Zhu, B. Adebisi, G. Gui, H. Gacanin, and F. Adachi, "NAS-AMR: Neural architecture search-based automatic modulation recognition for integrated sensing and communication systems," *IEEE Transactions on Cognitive Communications and Networking*, vol. 8, no. 3, pp. 1374-1386, 2022.
- [27] M. Du, X. He, X. Cai, and D. Bi, "Balanced neural architecture search and its application in specific emitter identification," *IEEE Transactions on Signal Processing*, vol. 69, pp. 5051-5065, 2021.
- [28] X. Zhang, X. Zhou, M. Lin, and J. Sun, "ShuffleNet: An extremely efficient convolutional neural network for mobile devices," in *Proc. IEEE/CVF Conf. Computer Vision and Pattern Recognition (CVPR)*, Los Alamitos, CA, USA, Jun. 2018, pp. 6848-6856.
- [29] N. Ma, X. Zhang, H.-T. Zheng, and J. Sun, "ShuffleNet V2: Practical guidelines for efficient CNN architecture design," in *Proc. European Conf. Computer Vision (ECCV)*, Munich, Germany, Sep. 2018, pp. 116-131.
- [30] J. Yin, L. Guo, W. Jiang, S. Hong, and J. Yang, "ShuffleNet-inspired lightweight neural network design for automatic modulation classification methods in ubiquitous IoT cyber-physical systems," *Computer Communications*, vol. 176, pp. 249-257, 2021.
- [31] H.-I. Choi and W. J. Williams, "Improved time-frequency representation of multicomponent signals using exponential kernels," *IEEE Transactions on Acoustics, Speech, and Signal Processing*, vol. 37, no. 6, pp. 862-871, Jun. 1989.
- [32] L. Sifre, "Rigid-motion scattering for image classification," Ph.D. dissertation, Ecole Polytechnique, CMAP, Oct. 2014.
- [33] S. Ioffe and C. Szegedy, "Batch normalization: Accelerating deep network training by reducing internal covariate shift," in *Proc. 32nd Int. Conf. Machine Learning (ICML)*, Lille, France, Jul. 2015, pp. 448-456.
- [34] V. Nair and G. E. Hinton, "Rectified linear units improve restricted Boltzmann machines," in *Proc. 27th ICML*, Haifa, Israel, Jun. 2010, pp. 807-814.
- [35] K. He, X. Zhang, S. Ren, and J. Sun, "Deep residual learning for image recognition," in *Proc. IEEE Conf. Computer Vision and Pattern Recognition (CVPR)*, Las Vegas, NV, USA, Jun. 2016, pp. 770-778.
- [36] R. R. Selvaraju, M. Cogswell, A. Das, R. Vedantam, D. Parikh, and D. Batra, "Grad-CAM: Visual explanations from deep networks via gradient-based localization," in *Proc. IEEE Int. Conf. Computer Vision (ICCV)*, Venice, Italy, Oct. 2017, pp. 618-626.
- [37] D. P. Kingma and J. Ba, "Adam: A method for stochastic optimization," in *Proc. 3rd Int. Conf. Learning Representations (ICLR)*, San Diego, CA, USA, May 2015.
- [38] *USRP N200/N210 Networked Series*. Ettus Research, Mountain View, CA, USA, 2012. [Online]. Available: https://www.ettus.com/wp-content/uploads/2019/01/07495_Ettus_N200-210_DS_Flyer_HR_1.pdf